npj | precision oncology

Article

Published in partnership with The Hormel Institute, University of Minnesota

https://doi.org/10.1038/s41698-025-01169-0

Siglec-14-LGALS3BP glycoimmune axis shapes tumor-associated macrophage polarization and confers poor outcome in colorectal cancer

Kuan-Yu Lin[1,8], Jeng-Kai Jiang[2,3,8], Jui-I Lai[1], Si-Yun Lin[1], Yu-Chang Ku[1], Miao-Hsia Lin[1], Chih-Yung Yang[4,5], Liang-Chuan Lo[6], Tsui-Ling Hsu[7] & Yung-Chi Chang[1] ✉

Colorectal cancer (CRC) is a leading cause of cancer-related deaths, particularly in metastatic cases. Sialic acid, frequently overexpressed in tumors, promotes immune evasion by engaging Siglecs (Sialic acid-binding immunoglobulin-like lectins) on immune cells. Siglec-5 and Siglec-14, expressed on myeloid cells, share ligand-binding domains but have opposing signaling functions. While these paired receptors regulate macrophage immune responses against bacterial infection, their role in the tumor microenvironment remains unclear. We found that Siglec-14 expression in THP-1 macrophages, when exposed to CRC tumor-conditioned medium, induces a protumoral SPP1^{+} tumor-associated macrophage phenotype, with enrichment of angiogenic pathways. In vivo, Siglec-14-expressing macrophages promoted CRC xenograft growth in mice, and their conditioned medium enhanced angiogenesis in chicken chorioallantoic membranes. We identified LGALS3BP (Lectin galactoside-binding soluble 3 binding protein), a sialylated glycoprotein in CRC tumor-conditioned medium, as a Siglec-14 ligand. Blocking this interaction reduced tumor-associated macrophage polarization and VEGF release. Siglec-14 is absent in some individuals due to a *SIGLEC5/14* fusion polymorphism. Siglec-14-positive CRC patients exhibited elevated serum LGALS3BP, which correlated with advanced progression and poorer survival. Collectively, these findings establish the LGALS3BP-Siglec-14 axis as a potential therapeutic target, offering a strategy to enhance antitumor immunity in Siglec-14-positive CRC patients.

Colorectal cancer (CRC) is the third most prevalent cancer and the second leading cause of cancer-related deaths worldwide, with ~1.8 million new cases and 940,000 deaths annually. Despite treatment advances, metastatic CRC retains a poor prognosis, with a 5-year survival rate of 15% for stage IV patients, who account for 22% of diagnoses[1,2]. One key hallmark of malignant transformation is aberrant glycosylation, notably increased sialylation, which promotes tumor progression through metastasis, angiogenesis, immune evasion, and chemoresistance—all major contributors to poor outcomes[3–5].

Tumor-associated sialoglycans regulate immune responses by interacting with sialic acid (Sia)-binding immunoglobulin-like lectins (Siglecs) on immune cells, including T cells, NK cells, macrophages, and dendritic cells. This interaction forms a glyco-immune checkpoint within the tumor microenvironment (TME), promoting immune suppression[5–7]. Most Siglecs, from Siglec-2 (CD22) to Siglec-XII, feature cytosolic immunoreceptor tyrosine-based inhibitory motif (ITIM) or ITIM-like domains that suppress immune responses. In contrast, a subset, including

[1]Graduate Institute of Microbiology, College of Medicine, National Taiwan University, Taipei, 10051, Taiwan. [2]School of Medicine, National Yang Ming Chiao Tung University, Taipei, 112304, Taiwan. [3]Division of Colon & Rectal Surgery, Department of Surgery, Taipei Veterans General Hospital, Taipei, 112304, Taiwan. [4]General Education Center, University of Taipei, Taipei, 100234, Taiwan. [5]Department of Education and Research, Taipei City Hospital, Taipei, 10629, Taiwan. [6]Cancer and Immunology Research Center, National Yang Ming Chiao Tung University, Taipei, 112304, Taiwan. [7]Genomics Research Center, Academia Sinica, Taipei, Taiwan. [8]These authors contributed equally: Kuan-Yu Lin, Jeng-Kai Jiang. ✉e-mail: yungchiychang@ntu.edu.tw

Siglec-14, -15, and -16, pairs with the adapter protein DNAX activation protein of 12 kDa (DAP12), which contains an immunoreceptor tyrosine-based activation motif (ITAM) to boost immune activity[8,9].

ITIM-bearing Siglecs, such as Siglec-7 and -9, inhibit $CD8^+$ T cell and NK cell cytotoxicity and skew macrophages toward immunosuppressive, tumor-promoting phenotypes[10–16]. Engagement of Siglec-9 and Siglec-10 also hampers macrophage-mediated tumor clearance[17,18]. Meanwhile, the roles of DAP12-associated Siglecs in cancer are less clear. Siglec-15 promotes immunosuppressive cytokine production in macrophages, and blocking it boosts antitumor immunity and curbs bone metastases[19–22]. Siglec-16, however, facilitates M1 macrophage polarization, and was linked to improved survival in glioblastoma patients[23]. Siglec-5 and Siglec-14, expressed on myeloid cells, are paired receptors that share identical sialoglycan-binding properties but opposing effects. Siglec-5 suppresses immune responses via its ITIM domain, while Siglec-14 amplifies activation through DAP12[9,24]. A genetic fusion between *SIGLEC5* and *SIGLEC14* causes a *SIGLEC14*-null polymorphism with geographic variation, affecting antibacterial and inflammatory responses[25–27]. However, the role of this paired receptor system in the TME remains unexplored.

This study examines the immunomodulatory effect of Siglec-5/-14 in the CRC TME. We showed that Siglec-14 steers macrophage polarization to a $SPP1^+$ tumor-associated macrophage (TAM) phenotype, which is associated with tumor progression. We also pinpointed lectin galactoside-binding soluble 3 binding protein (LGALS3BP), a highly sialylated protein, as a key ligand for Siglec-5/-14 in CRC. Elevated serum LGALS3BP levels correlated with worse clinical outcomes, underscoring the potential importance of the LGALS3BP-Siglec-14 axis in CRC progression.

Results

Siglec-14 promotes macrophage polarization to the M2/TAM phenotype

To explore the immunomodulatory role of the Siglec-5/-14 paired receptor in macrophage polarization, human monocytic THP-1 cells were engineered to express either vector control (EV/THP-1), human Siglec-5 (S5/THP-1), or human Siglec-14 (S14/THP-1). Expression of Siglec-5 and Siglec-14 was confirmed by flow cytometry (Supplementary Fig. 1). Following differentiation with PMA and polarization with LPS/IFN-γ (M1) or IL-4/IL-13 (M2), we measured M1 and M2 marker levels. Pro-inflammatory cytokine transcripts (*TNF*, *IL1B*, and *IL6*) and their corresponding proteins showed marginal differences across groups (Fig. 1A, C). However, Siglec-14 markedly upregulated M2 marker transcripts (*CCL22*, *CD204*, *LXRA*, and *PPARG*) and CCL22 protein levels compared to EV/THP-1 and S5/THP-1 macrophages ($P < 0.01$, Fig. 1B, C), suggesting a tilt toward M2 polarization.

Tumors release signals that shape immune cells in the TME, driving angiogenesis and tolerance. To test whether Siglec-14 amplifies TAM polarization in response to cancer-derived factors, we exposed PMA-differentiated THP-1 macrophages to tumor-conditioned medium (TCM) from human CRC SW620 cells (TCM^{SW620}) for 48 h. Pro-inflammatory cytokine transcripts (*TNF* and *IL6*) showed no significant increase after TCM^{SW620} treatment. In contrast, TAM markers (*PD-L1*, *IL10*, *CCL17*, *CCL22*, *VEGFA*, and *TGFB*) were significantly elevated in S14/THP-1 macrophages compared to EV/THP-1 and S5/THP-1 macrophages (Fig. 1D). Consistently, CCL22 and VEGF protein levels were markedly increased in supernatants of TCM^{SW620}-treated S14/THP-1 macrophages (Fig. 1E). Similar findings were observed using TCM from other CRC cell lines (HT29, DLD-1, and HCT116), as indicated by increased *CCL17* and *VEGFA* levels (Fig. 1F), suggesting a broader role for Siglec-14 in fostering TAM polarization.

Siglec-14 drives $SPP1^+$ TAM signatures in TCM^{SW620}-treated macrophages

To investigate the role of Siglec-14 in modulating the transcriptomic profile of TCM-treated THP-1 macrophages, we exposed EV/THP-1, S5/THP-1, and S14/THP-1 macrophages to TCM^{SW620} for 48 h, followed by bulk RNA sequencing. We analyzed differentially expressed genes (DEGs) across these groups, both with and without TCM^{SW620} treatment, using k-means clustering with k = 6 (Fig. 2A and Supplementary Data 1). Gene clusters were subjected to Gene Ontology (GO) enrichment analysis, with the most significantly enriched GO terms (FDR <0.01) shown in Fig. 2B. Notably, cluster 3, comprising genes upregulated in S14/THP-1 macrophages treated with TCM^{SW620}, was enriched in biological processes related to cell adhesion, migration, inflammatory response, and angiogenesis (Fig. 2B), suggesting a tumor-supportive role for Siglec-14.

Recent studies utilizing single-cell RNA sequencing have identified two distinct TAM phenotypes in CRC: $C1QC^+$ TAMs, which are correlated with favorable prognosis, and $SPP1^+$ TAMs, which are associated with poorer clinical outcomes[28,29]. $SPP1^+$ TAMs are characterized by enriched pathways that promote angiogenesis, extracellular matrix-receptor interactions, and tumor vasculature development, whereas $C1QC^+$ TAMs are linked to complement activation and antigen presentation. To evaluate whether Siglec-14 drives macrophage polarization toward the $SPP1^+$ TAM phenotype, we compared gene expression profiles of mock- and TCM^{SW620}-treated EV/THP-1, S5/THP-1, and S14/THP-1 macrophages using the $C1QC^+$ and $SPP1^+$ TAM gene signatures defined by ref. 28. Our analysis demonstrated that both mock- and TCM^{SW620}-treated S14/THP-1 macrophages exhibited significantly higher expression of $SPP1^+$ TAM signature genes and lower expression of $C1QC^+$ TAM markers. Despite Siglec-14 alone induced some TAM-associated gene changes but our data still demonstrated that Siglec-14 can further amplified TCM^{SW620}-driven TAM polarization (Fig. 2C, with the complete gene list and their TPM value in Supplementary Data 2). These results were validated by RT-qPCR (Fig. 2D). Furthermore, Gene Set Enrichment Analysis (GSEA) revealed that pathways associated with $SPP1^+$ TAMs, such as angiogenesis, vasculature development, epithelial development, and positive regulation of cell migration, were significantly enriched in TCM^{SW620}-treated S14/THP-1 macrophages compared to TCM^{SW620}-treated S5/THP-1 macrophages (Fig. 2E). Collectively, these results indicate that Siglec-14 promotes the development of a tumor-supportive $SPP1^+$ TAM phenotype in macrophages exposed to CRC TCM.

Siglec-14 enhances macrophage-mediated tumor-promoting and angiogenic activities

To investigate whether Siglec-14-mediated macrophage polarization contributes to CRC progression, we co-inoculated SW620 tumor cells with THP-1 macrophages into nude mice (Fig. 3A). The co-inoculation of macrophages with tumor cells led to increased tumor volume and weight compared to tumors formed by SW620 cells alone. Notably, S14/THP-1 macrophages promoted faster and larger tumor growth than either EV/THP-1 or S5/THP-1 macrophages (Fig. 3B–D). This enhanced tumorigenicity did not result from differences in macrophage proliferation, as PMA-differentiated THP-1 macrophages did not proliferate, and cell numbers remained comparable across all experimental groups after 2 days of culture (Fig. 3E).

TAMs secrete a range of cytokines, chemokines, growth factors, and metabolites that support tumor growth, reduce cell death, and promote angiogenesis. To assess the functional role of Siglec-14 in these processes, we evaluated the effects of conditioned medium from TCM^{SW620}-treated macrophages (MφCM) on CRC cells. However, MφCM derived from EV/THP-1, S5/THP-1, and S14/THP-1 macrophages had no impact on the growth rate, sensitivity to 5-fluorouracil, or clonogenicity and sphere formation of CRC cells (Supplementary Fig. 2A–F). Given the significant increase in VEGF, a key pro-angiogenic factor, in S14/THP-1 following stimulation with CRC TCM, we next examined the effects of MφCM on endothelial cell behavior. MφCM from mocked-treated S14/THP-1 macrophage had only minimal effects on the survival and migration of human umbilical vein endothelial cell (HUVEC), whereas MφCM from TCM^{SW620}-treated S14/THP-1 macrophages ($MφCM^{S14/THP-1}$) markedly enhanced both processes compared with MφCM from TCM^{SW620}-treated EV/

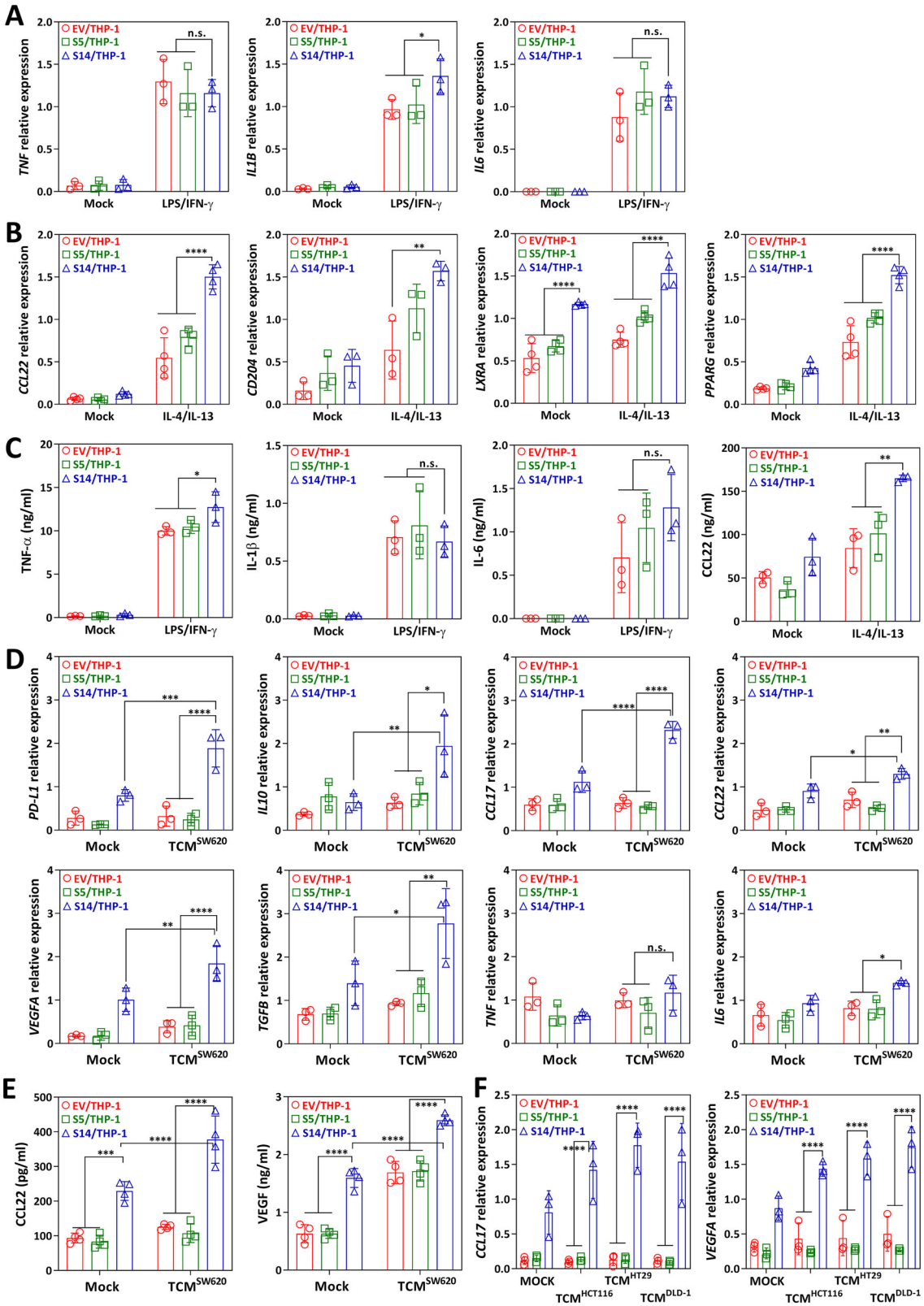

Fig. 1 | Siglec-14 potentiates M2-like TAM polarization. **A** RT-qPCR analysis of mRNA levels of M1 macrophage markers in THP-1 macrophages treated with LPS/IFN-γ. **B** RT-qPCR analysis of mRNA levels of M2 macrophage markers in THP-1 macrophages treated with IL-4/IL-13. **C** Protein levels of TNF-α, IL-1β, IL-6, and CCL22 in the culture supernatants from stimulated THP-1 macrophages were analyzed by ELISA. **D** Transcript levels of TAM-associated markers in THP-1 macrophages treated with TCM^{SW620}. **E** Production of CCL22 and VEGF in the culture supernatants of TCM^{SW620}-stimulated THP-1 macrophages was determined by ELISA. **F** RT-qPCR analysis of mRNA levels of *CCL17* and *VEGFA* in THP-1 macrophages treated with TCM from HCT116, HT29 and DLD-1 cells. Data were normalized with *HPRT1* and presented as mean ± SD from 3 to 4 independent experiments (**A**, **B**, **D**, **F**). Significance was determined by two-way ANOVA with Tukey's multiple comparison post hoc test. $^{*}P < 0.05$; $^{**}P < 0.01$; $^{***}P < 0.001$; $^{****}P < 0.0001$; n.s., not significant.

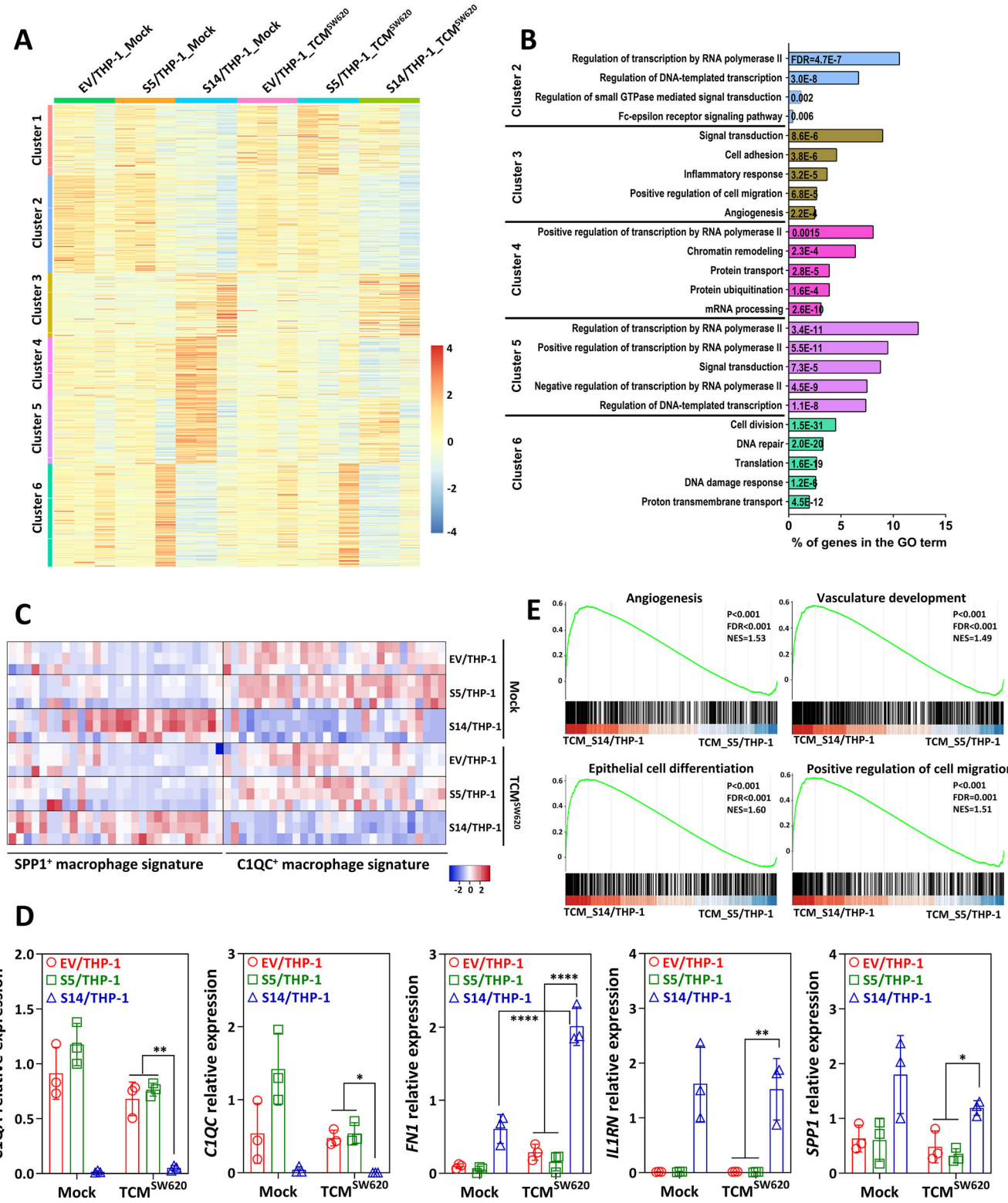

Fig. 2 | Transcriptomic analysis of TCM^{SW620}-treated THP-1 macrophages. **A** Heatmap of k-means clustering of variably expressed genes in EV/THP-1, S5/THP-1, and S14/THP-1 macrophages with or without TCM^{SW620} treatment ($n = 16{,}918$, $k = 6$). Genes were grouped into six clusters on the basis of expression similarity. **B** GO enrichment analysis of genes in each cluster using DAVID, showing top enriched GO terms with a FDR <0.01. **C** A Heatmap of gene expression levels of SPP1$^+$ and C1QC$^+$ macrophage signature in mock- and TCM^{SW620}-treated EV/THP-1, S5/THP-1, and S14/THP-1 macrophages. **D** RT-qPCR analysis of mRNA levels of indicated genes in mock- and TCM^{SW620}-treated THP-1 macrophages. Data were normalized with *HPRT1* and presented as mean ± SD from three independent experiments. Significance was determined by two-way ANOVA with Tukey's multiple comparison post hoc test. $^*P < 0.05$; $^{**}P < 0.01$; $^{****}P < 0.0001$. **E** GSEA showing upregulated genes related to angiogenesis, vasculature development, epithelial development, and positive regulation of cell migration in TCM^{SW620}-treated S14/THP-1 macrophages compared to TCM^{SW620}-treated S5/THP-1 macrophages.

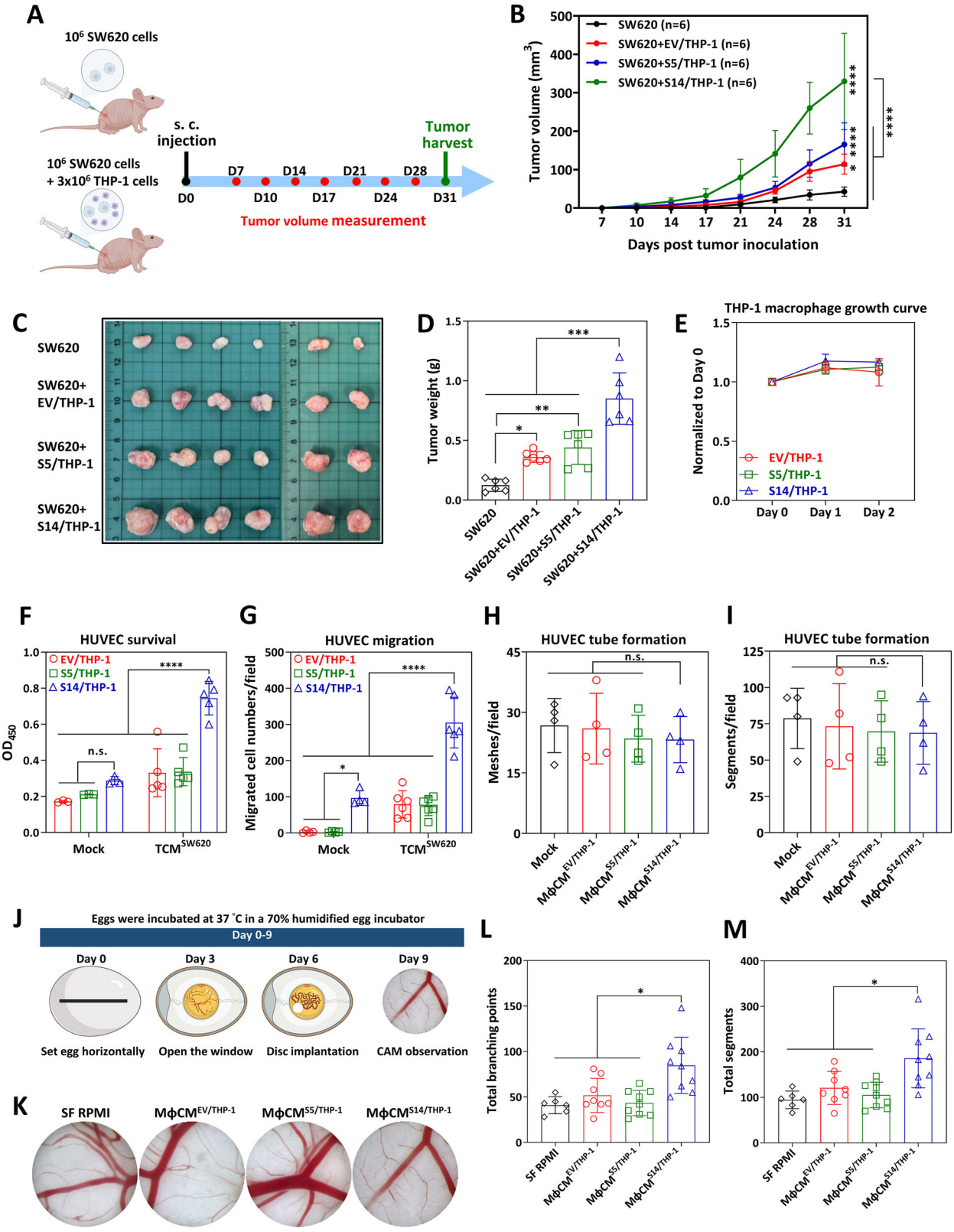

THP-1 macrophages ($M\varphi CM^{EV/THP-1}$) or S5/THP-1 macrophages ($M\varphi CM^{S5/THP-1}$) (Fig. 3F, G). $M\varphi CM^{S14/THP-1}$ did not increase tubulogenesis in an in vitro Matrigel angiogenesis assay (Fig. 3H, I), likely due to short exposure and the strong intrinsic angiogenic activity of Matrigel. In a chicken chorioallantoic membrane (CAM) model with extended treatment duration (Fig. 3J), $M\varphi CM^{S14/THP-1}$ significantly increased capillary formation, branching points, and vessel segments relative to controls (Fig. 3K–M). These results demonstrated that Siglec-14 enhances the pro-angiogenic functions of TAMs in response to CRC-derived factors.

Fig. 3 | Siglec-14 enhances macrophage-mediated pro-tumorigenic and pro-angiogenic functions. **A** Experimental design of the SW620 xenograft model in nude mice (Created with BioRender.com). Mice were subcutaneously implanted with SW620 cells alone or mixed with PMA-differentiated THP-1 macrophages into the right flank. **B** Tumor volumes in xenografted mice over time. **C** Photographs of xenograft tumors on day 31 post-implantation. **D** Weights of solid tumors on day 31 post-implantation. **E** WST-1 assay to determine the proliferation of PMA-differentiated THP-1 cells. **F** WST-1 assay of HUVEC viability 48 h after MφCM exposure. Data were expressed as mean ± SD from 3 to 5 independent experiments. **G** HUVEC migration assay. HUVECs were exposed to MφCM for 24 h, and migrated cells were stained with crystal violet and counted under a microscope. Data were expressed as mean ± SD from 4 to 6 independent experiments. **H**, **I** In vitro angiogenesis assay. HUVECs were cultured with MφCM on a Matrigel-coated plate for 6 h. Tube meshes (**H**) and segments (**I**) were quantified using ImageJ software. Data were expressed as mean ± SD from two independent experiments with biological duplicates. **J** Graphic illustration of the experimental procedure for CAM assay (Created with BioRender.com). **K** Representative CAMs at EDD 9 are shown for each treatment. The number of vessel branching points (**L**) and segments (**M**) in each CAM were quantified using WimCAM analysis, and presented as mean ± SD ($n = 6–9$ for each group). Significance was determined by one-way ANOVA (**D**, **H**, **I**, **L**, **M**) or two-way ANOVA (**B**, **F**, **G**) with Tukey's multiple comparison post hoc test. $^{*}P < 0.05$; $^{**}P < 0.01$; $^{***}P < 0.001$; $^{****}P < 0.0001$; n.s., not significant.

Identification of Siglec-14 ligands and elucidation of their role in TAM polarization

Siglec-14 activation involves interaction with the ITAM-containing DAP12 adapter and spleen tyrosine kinase (SYK)-dependent signaling[24]. In PMA-differentiated S14/THP-1 macrophages, phosphorylated SYK levels were significantly higher compared to EV/THP-1 and S5/THP-1 macrophages, even without TCM^{SW620} stimulation (Fig. 4A), indicating constitutive SYK activation in Siglec-14-expressing cells post-PMA differentiation. Pre-treatment with SYK inhibitor Bay 61-3606 (Fig. 4B) or Siglec-14 neutralizing antibodies (Fig. 4C) markedly reduced CCL22 and VEGF production in S14/THP-1 macrophages upon TCM^{SW620} exposure, highlighting the critical role of Siglec-14 and SYK in TAM polarization.

To explore Siglec-14 interactions with tumor-associated sialoglycans in TCM^{SW620}, we incubated TCM^{SW620} with wild-type Siglec-5 and Siglec-14 ($S5^{WT}$-Fc and $S14^{WT}$-Fc) or their Sia-binding-deficient mutants carrying the R119A substitution ($S5^{R119A}$-Fc and $S14^{R119A}$-Fc). The conserved arginine residue (R119) in the V-set domain is critical for Sia recognition[30]. TCM^{SW620} sialoglycans bound to $S5^{WT}$-Fc and $S14^{WT}$-Fc but not to their R119A mutants (Fig. 4D), confirming the interaction is Sia-dependent. Consistently, multiple sialylated complex-type glycans were identified in TCM^{SW620} (Supplementary Fig. 3A).

To identify Sia-dependent ligands of Siglec-14, TCM^{SW620} was incubated with protein A beads immobilized with $S14^{WT}$-Fc and $S14^{R119A}$-Fc. Silver-stained SDS-PAGE analysis revealed distinct protein bands unique to $S14^{WT}$-Fc (Supplementary Fig. 3B). Mass spectrometry identified Lectin galactoside-binding soluble 3 binding protein (LGALS3BP, also known as Gal-3BP, 90 K or Mac-2BP) as the top candidate ligand (Supplementary Data 3). Immunoprecipitation-western blot analysis confirmed Sia-dependent binding of LGALS3BP to $S14^{WT}$-Fc, with no binding to $S14^{R119A}$-Fc (Fig. 4E). Siglec-5 showed similar binding specificity (Supplementary Fig. 3C). The secreted form of LGALS3BP (arrow, Fig. 4E) migrated at a higher molecular weight than its intracellular form (arrowhead) and was recognized by the α-2,6 Sia-binding *Sambucus nigra* lectin (SNA) (Fig. 4F), indicating that sialylation of LGALS3BP is critical for Siglec-5/-14 recognition. To further test this, we generated CMAS (cytidine monophosphate-N-acetylneuraminic acid synthase) knockout (KO) SW620 cells, eliminating the activated Sia donor required for sialyltransferases (Supplementary Fig. 3D). Conditioned medium from CMAS KO or sialyltransferase inhibitor P-3Fax-Neu5Ac-treated cells contained LGALS3BP with reduced molecular weight and lost Siglec-14 binding, mimicking the $S14^{R119A}$ mutant (Supplementary Fig. 3E). These findings demonstrate that sialylated glycans on LGALS3BP are essential for Siglec-14 interaction.

LGALS3BP was abundantly detected in TCM from multiple CRC cell lines, with significantly higher levels than in conditioned medium from normal colonic epithelial CCD 841 CoN cells (Supplementary Fig. 3F). To assess its role in TAM polarization, we generated LGALS3BP KO SW620 cells (Fig. 4G). TCM from LGALS3BP KO cells induced significantly lower expression of TAM markers (CCL22, VEGF) in S14/THP-1 macrophages compared with WT TCM, at both mRNA and protein levels (Fig. 4H, I). In addition, recombinant LGALS3BP enhanced IL-4/IL-13-induced M2 gene expression (*CCL17* and *CCL22*) in a dose-dependent manner (Supplementary Fig. 3G, H). Together, these findings demonstrate that the Siglec-14-LGALS3BP axis potentiates M2/TAM polarization.

Serum LGALS3BP, *SIGLEC14* genotype, and clinical outcomes

To evaluate the clinical relevance of the LGALS3BP-Siglec-14 axis in CRC, we analyzed serum LGALS3BP levels and *SIGLEC14* genotypes in 357 CRC patient specimens using enzyme-linked immunosorbent assay (ELISA) and genomic PCR, respectively. CRC patients were stratified into high and low serum LGALS3BP level groups using the median serum LGALS3BP concentration as the cut-off threshold. The same cohort was further categorized as Siglec-14 positive or negative based on the presence or absence of the *SIGLEC14* gene (Fig. 5A). The associations between serum LGALS3BP levels, *SIGLEC14* genotypes, and clinicopathological characteristics of CRC patients were examined and summarized in Table 1. Serum LGALS3BP levels showed no significant correlation with age, gender, T stage, differentiation status, tumor location, or carcinoembryonic antigen (CEA) and carbohydrate antigen 19-9 (CA19-9) levels. However, serum LGALS3BP levels were significantly associated with pathological tumor/node/metastasis (TNM) stage, microsatellite instability (MSI) status, immune cell infiltration, lymphatic invasion, and *SIGLEC14* genotype (all $p < 0.05$). Additionally, a weak correlation was observed between serum LGALS3BP levels and vascular invasion ($p = 0.0572$).

Further analysis of serum LGALS3BP levels across clinicopathological subgroups revealed that higher serum LGALS3BP levels were significantly correlated with advanced TNM stages (Fig. 5B and Supplementary Fig. 4A–C). Moreover, serum LGALS3BP levels were markedly higher in microsatellite stable (MSS) CRC patients, often referred as "cold tumors" due to their typically poor responses to immunotherapy[31,32] (Fig. 5C). Additionally, serum LGALS3BP levels were significantly elevated in patients with lymphatic and vascular invasion (Fig. 5D, E) and in those with reduced immune cell infiltration (Fig. 5F). While the *SIGLEC14*-null polymorphism did not significantly correlate with CRC clinicopathological characteristics (data not shown), *SIGLEC14* positive CRC patients exhibited higher serum LGALS3BP levels than their *SIGLEC14* negative counterparts (Fig. 5G).

We further examined the association between serum LGALS3BP levels and CRC patient survival. As shown in Fig. 5H, CRC patients with high serum LGALS3BP levels had significantly lower CRC-specific survival rates than those with low serum LGALS3BP levels across all I-IV stages. Multivariate Cox regression analysis identified serum LGALS3BP levels as an independent predictive biomarker for poor prognosis in CRC after adjusting for covariates (Table 2, hazard ratio [HR] 5.948, 95% confidence interval [CI] 1.899–18.630, $p = 0.002$). In summary, our retrospective study demonstrated that Siglec-14-positive CRC patients exhibit higher serum LGALS3BP levels, which are significantly associated with advanced TNM stage, increased vascular and lymphatic invasion, and CRC progression. These findings suggest that serum LGALS3BP could serve as a potential prognostic biomarker for poor clinical outcomes in CRC patients.

Discussion

Siglecs are a family of cell-surface receptors predominantly expressed on immune cells. Most Siglecs possess ITIMs in their cytoplasmic domains, enabling them to function as inhibitory receptors. Elevated levels of these

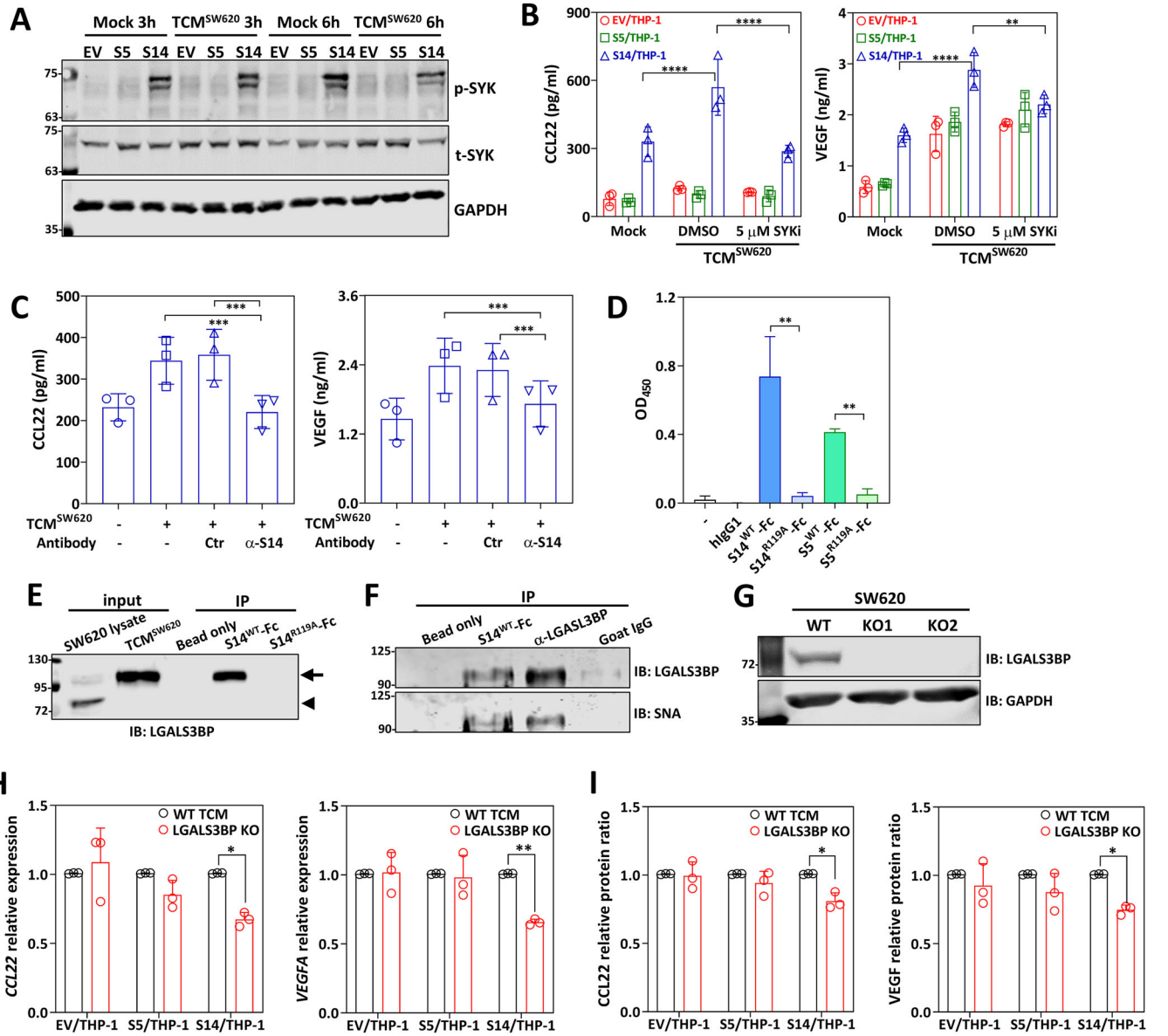

Fig. 4 | The LGALS3BP-Siglec-14 axis drives TAM polarization. A Western blot analysis of SYK phosphorylation (p-SYK) in TCM^{SW620}-treated THP-1-macrophages, with total SYK (t-SYK) and GAPDH as a loading control. **B**, **C** ELISA quantification of CCL22 and VEGF production in TCM^{SW620}-stimulated THP-1 macrophages treated with either a SYK inhibitor (**B**) or Siglec-14 neutralizing antibodies (**C**). Data were expressed as mean ± SD from three independent experiments. **D** Interaction of TCM^{SW620} with different Siglec-Fc was determined by ELISA. Data were expressed as mean ± SD from two independent experiments with biological triplicate. **E**, **F** TCM^{SW620} was immunoprecipitated with Siglec-Fc or anti-LGALS3BP antibodies, followed by immunoblotting with anti-LGALS3BP antibodies (**E**) or *Sambucus nigra* agglutinin (SNA) (**F**). **G** Western blot analysis of LGALS3BP expression in WT and LGALS3BP KO SW620 cells. **H** RT-qPCR analysis of mRNA levels of *CCL22* and *VEGFA* in THP-1 macrophages exposed to WT TCM or LGALS3BP KO TCM. Data were normalized with *HPRT1* and presented as mean ± SD from three independent experiments. **I** Production of CCL22 and VEGF in THP-1 macrophages exposed to WT TCM or LGALS3BP KO TCM, determined by ELISA. Data were expressed as mean ± SD from three independent. Significance was determined by one-way ANOVA with Tukey's multiple comparison post hoc test. $^{*}P < 0.05$; $^{**}P < 0.01$; $^{***}P < 0.001$; $^{****}P < 0.0001$.

inhibitory Siglecs have been reported in tumor-infiltrating immune cells across multiple cancer types[12,16,21,33–36]. Within the TME, the interaction of Siglecs with sialylated ligands triggers tolerogenic signaling cascades that suppress T and NK cell activation and cytotoxicity[12–14,16,37,38]. Furthermore, Siglec signaling promotes macrophage polarization toward protumoral phenotypes while impairing their phagocytosis and antigen presentation functions[10,11,15,17,18,39–41].

Desialylation of tumor cells has been shown to enhance anti-cancer immune responses[38,42–44]. However, a more targeted approach involves identifying specific Siglec ligands upregulated in malignant cells that selectively engage dominant Siglec receptors on immune cells. In this study, we used immunoprecipitation-mass spectrometry to identify LGALS3BP as a key Sia-dependent ligand for Siglec-14 in CRC TCM (Fig. 4E and Supplementary Data 3). Siglecs generally exhibit low affinity for sialylated glycoconjugates, with dissociation constants (Kd) ranging from 0.1 to 3 mM[9]. However, LGALS3BP, a highly N-glycosylated secreted glycoprotein, forms high-molecular-mass oligomers exceeding 1000 kDa[45–49], which substantially increases its avidity for Siglecs. LGALS3BP has previously been shown to interact with multiple inhibitory Siglecs, including Siglec-5, -6, -7, -9, -10, and -11, and its binding to Siglec-9 has been implicated in neutrophil-mediated tumor suppression[50]. Given that Siglec-5 and Siglec-14 differ by only a single amino acid in their first two domains, it has been

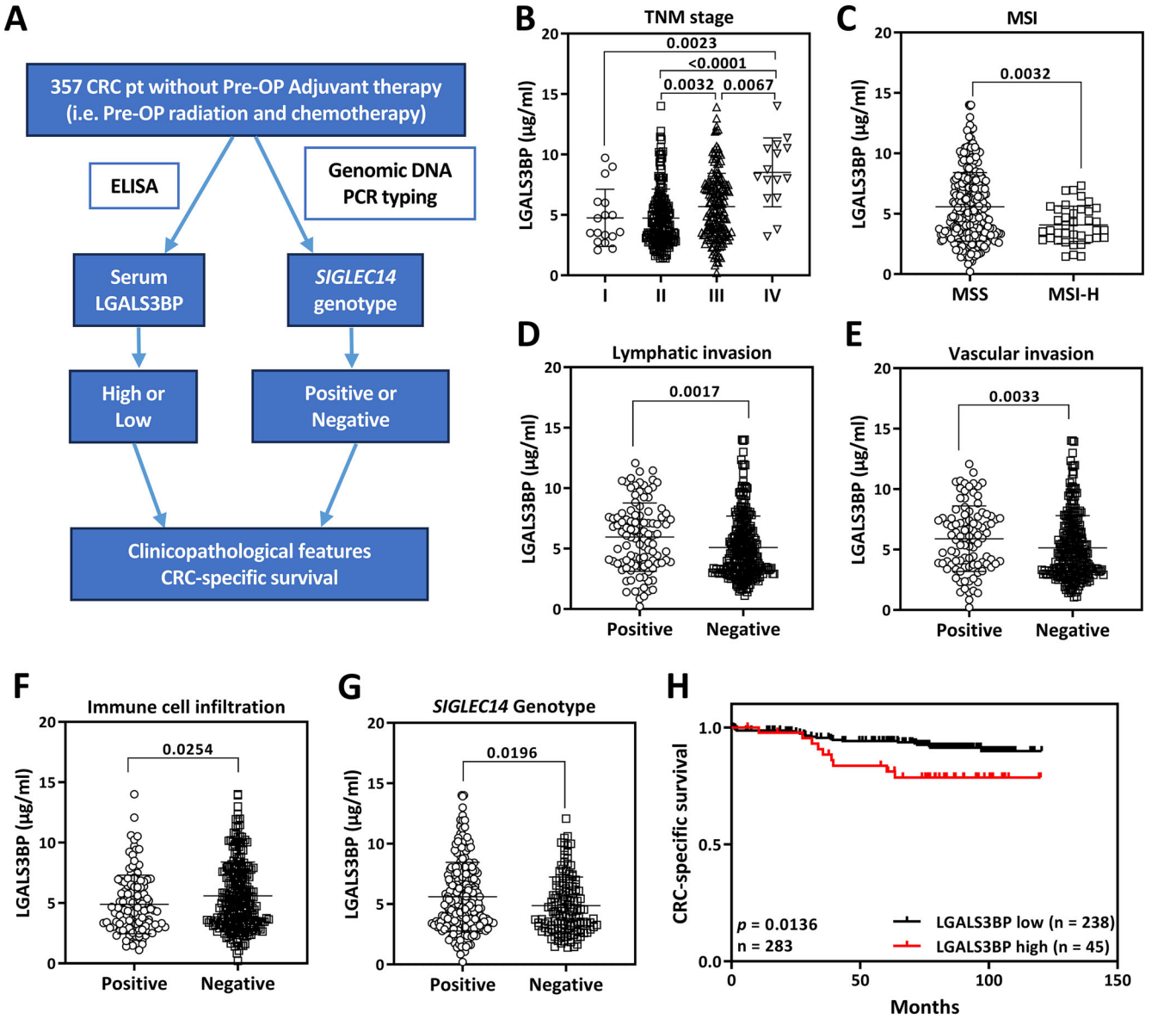

Fig. 5 | Serum LGALS3BP levels in CRC patients and correlation with clinicopathological features and patient survival. A Flow chart of patient inclusion in this study. **B–G** Serum LGALS3BP levels in CRC patients, measured by ELISA, were analyzed based on tumor pathological stages (**B**), microsatellite instability (MSI) status (**C**), lymphatic invasion (**D**), vascular invasion (**E**), immune cell infiltration (**F**), and *SIGLEC14* genotype (**G**). **H** Kaplan–Meier curve showing CRC-specific survival in patients with high and low serum LGALS3BP levels. Significance was determined by one-way ANOVA with Dunn's multiple comparison post hoc test (**B**) or Mann–Whitney *U*-test (**C–G**).

hypothesized that LGALS3BP also binds Siglec-14. In this study, we confirmed this interaction and further uncovered a novel role of this interaction in promoting macrophage polarization toward a protumoral SPP1^{+} TAM phenotype (Fig. 2).

Recent studies have identified two distinct TAMs subsets in CRC, SPP1^{+} TAMs and C1QC^{+} TAMs. While C1QC^{+} TAMs are enriched in genes related to phagocytosis and antigen presentation, SPP1^{+} TAMs exhibit a protumoral and pro-angiogenic signature and engage in crosstalk with tumor-associated fibroblast and endothelial cells[28,29]. Consistent with these findings, S14/THP-1 macrophages treated with TCM^{SW620} showed significant enrichment of angiogenic and vasculature development pathways (Fig. 2E). Functionally, MφCM from TCM^{SW620}-treated S14/THP-1 macrophages enhanced HUVEC survival and migration, and promoted in vivo angiogenesis in the CAM model (Fig. 3J–M). We disrupted the LGALS3BP-Siglec-14 axis using three approaches: Siglec-14 blockade, inhibition of downstream spleen tyrosine kinase (SYK) activation, and knockout of LGALS3BP in SW620 cells. Each of these interventions significantly attenuated Siglec-14-mediated TAM polarization. Notably, these interventions also reduced the production of VEGF, a crucial angiogenic factor produced by SPP1^{+} TAMs (Fig. 4B, C, H, I). These findings suggest that targeting the LGALS3BP-Siglec-14 interaction could serve as a therapeutic strategy to modulate macrophage phenotype and enhance antitumor immunity in CRC.

Loss-of-function polymorphisms in *SIGLEC14* and *SIGLEC16* have been reported in human populations and are associated with reduced host immunity against bacterial infections[25–27,51–53]. Clinically, Siglec-14 overexpression correlates with poor prognosis in acute myeloid leukemia, whereas lower plasma Siglec-14 levels correlate with decreased risk of CRC[54,55]. In our cohort, however, the *SIGLEC14*-null polymorphism showed no significant association with patient survival. This lack of association may reflect complex regulatory mechanisms influencing Siglec-14 expression, localization, and function, which are not determined solely by

Table 1 | Correlation between the serum GAL3BP level with *SIGLEC14* genotype and the clinicopathological characteristics of CRC patients

	Case No. *N* = 357	LGALS3BP high *N* = 73	LGALS3BP low *N* = 284	*p* value
Age				
≥65	170	29	141	0.1489
<65	187	44	143	
Gender				
Male	191	34	157	0.191
Female	166	39	127	
T stage				
T1-T2	37	7	30	>0.9999
T3-T4	320	66	254	
N stage				
N0	177	24	153	**0.0058**
N1	115	32	83	
N2	65	17	48	
M stage				
M0	342	65	277	**0.0037**
M1	15	8	7	
Differentiation				
Poor	32	6	26	0.8725
Moderate	323	67	256	
Well	1	0	1	
Location				
Right colon	139	24	115	0.3547
Left colon	169	40	129	
Rectal	49	9	40	
CEA (ng/ml)				
> 5	146	33	113	0.425
≤ 5	211	40	171	
CA19-9 (U/ml)				
>37	54	12	42	0.7162
≤37	303	61	242	
MSI				
MSI-H	28	0	38	**0.0002**
MSS	273	65	208	
Immune cell infiltration				
Positive	141	16	125	**0.0005**
Negative	216	57	159	
Vascular invasion				
Positive	99	27	72	0.0572
Negative	257	46	211	
Lymphatic invasion				
Positive	106	30	76	**0.0213**
Negative	251	43	208	
SIGLEC14				
Positive	227	55	172	**0.0205**
Negative	130	18	112	

gene presence or absence. For example, *SIGLEC14* copy number variations affect mRNA expression levels, alternative splicing generates soluble forms of Siglec-14, and single-nucleotide polymorphisms (SNPs) within the *SIGLEC5*/*SIGLEC14* locus modulate vaccine-induced inflammatory responses[56–58]. A more integrative analysis combining *SIGLEC14*-null status, SNP variations, and Siglec-14 protein expression on TAMs may therefore provide a more accurate prediction of CRC progression.

The biology of LGALS3BP further adds complexity, as it interacts with multiple partners, including β1 integrins[45,59], galactins[60], endosialin[61], CD9/CD82 tetraspanin web[62], DC-SIGN[63], and Siglecs[50], exerting context-dependent effects. For example, LGALS3BP binding to galectin-3 and integrins enhances cell aggregation, migration and viability, thereby promoting metastasis[59], whereas its interaction with CD9/CD82 suppresses Wnt/β-catenin signaling and reduces cell proliferation, motility and tumorigenicity in nude mice[62]. It also modulates immune responses by engaging DC-SIGN to suppress dendritic cell maturation[63] and Siglec-9 to reduce neutrophil cytotoxicity[50]. Our study does not exclude contributions from these additional LGALS3BP-binding receptors. Nevertheless, our functional experiments provide direct evidence for a specific role of the Siglec-14-LGALS3BP axis in shaping the tumor microenvironment. Ectopic expression of Siglec-14 in THP-1 macrophages enhanced LGALS3BP-driven M2-like polarization, angiogenesis, and tumor-promoting effects, whereas these effects were absent in Siglec-5-expressing or control cells. Moreover, elevated circulating LGALS3BP levels were preferentially observed in Siglec-14-positive patients. Thus, while clinical outcomes likely reflect the combined effects of multiple LGALS3BP-receptor interactions, our mechanistic data highlight a distinct role for the Siglec-14-LGALS3BP axis in driving a protumoral macrophage phenotype within the CRC microenvironment.

Within the Siglec family, Siglec-5/Siglec-14 and Siglec-11/Siglec-16 are paired receptors characterized by similar ligand-binding specificities but divergent signaling outcomes. Our findings indicate that Siglec-14 expression on THP-1 macrophages significantly enhances M2/TAM polarization and accelerates the growth of xenografted SW620 cells, whereas Siglec-5 expression has a minimal effect compared to control THP-1 macrophages (Figs. 1 and 3A–D). Interestingly, recent studies have shown that Siglec-16 drives M1 macrophage polarization, promoting pro-inflammatory responses, whereas Siglec-11 suppresses inflammation and fosters M2 polarization[23,33,64]. These functional disparities likely arise from differences in assay system, ligand specificity, and receptor modulation by *cis*-ligands present on the same cell surface. Siglecs engage both Sias on the same cell surface (*cis*-ligands) and those present on other cells or pathogens (*trans*-ligands). Binding to *cis*-ligands can modulate Siglec function by restricting access to *trans*-ligands and altering the activity of *cis*-ligand-bearing receptors[9,65,66]. Notably, Siglec-11 and Siglec-16 selectively recognize α2-8-linked oligo- and polySias, predominantly found in neural tissues, whereas Siglec-5 and Siglec-14 recognize a broader range of ligands, including α2,3-, α2,6-, and α2,8-linked Sias, as well as protein and lipid-based ligands[67–70]. The negligible effect of Siglec-5 in our experimental model may stem from pronounced *cis*-ligand masking, which likely diminishes its responsiveness to external ligands. This differential regulation underscores the complexity of Siglec-mediated immune modulation in the TME.

A key limitation of this study is the lack of homologous genes for the human Siglec-5/Siglec-14 paired receptors in mice, which significantly hinders the investigation of their roles and the impact of *SIGLEC14* polymorphisms in animal models. Establishing lineage-specific expression of Siglec-5 and Siglec-14 in murine myeloid cells could provide valuable insights into the molecular mechanisms governing this primate-specific Siglec receptor pair.

In conclusion, this study identifies LGALS3BP as a tumor-associated sialoglycoprotein positively correlated with poor clinical outcomes in CRC patients. Our findings provide molecular evidence that LGALS3BP is the most abundant Siglec-14-interacting glycoprotein in CRC TCM, potentiating protumoral and pro-angiogenic TAM features. Given the limited studies on DAP12-coupled activating Siglecs in the TME, our work suggests that targeting the LGALS3BP-Siglec-14 axis may offer a viable strategy for reprogramming protumoral macrophages in Siglec-14-positive CRC patients. However, further studies are needed to explore the therapeutic potential of blocking this interaction in preclinical and clinical settings.

Table 2 | Univariate and multivariate Cox regression analysis for CRC-specific survival

CRC-specific survival		Univariate			Multivariate	
Variable	HR	95% CI	*P* value	HR	95% CI	*p* value
Age (≧65 vs <65)	3.317	1.374–8.003	**0.008**	4.330	1.454–12.899	**0.008**
Gender (male vs female)	0.884	0.397–1.968	0.763	1.680	0.615–4.587	0.311
Stage (late vs early)	1.447	0.648–3.231	0.368	0.991	0.323–3.045	0.988
Differentiation (Poorly vs others)	4.485	1.859–10.823	0.001	5.704	1.737–18.733	**0.004**
Location (left vs right)	0.831	0.372–1.857	0.651	1.682	0.610–4.637	0.315
CEA (>5 vs ≦5)	4.364	1.808–10.534	**0.001**	2.764	0.866–8.824	0.086
CA19-9 (>37 vs ≦37)	4.626	2.022–10.585	**<0.001**	4.109	1.248–13.534	**0.020**
MSI (MSS vs MSI)	0.630	0.184–2.153	0.461	0.276	0.063–1.200	0.086
Round cell infiltration (positive vs negative)	1.019	0.446–2.330	0.964	1.043	0.379–2.867	0.935
Lymphatic invasion (positive vs negative)	3.402	1.523–7.599	**0.003**	1.328	0.452–3.904	0.606
SIGLEC14 (positive vs negative)	0.707	0.317–1.577	0.397	1.005	0.389–2.596	0.992
LGALS3BP (high vs low)	2.484	1.085–5.685	**0.031**	5.948	1.899–18.630	**0.002**

Methods

Cell lines

Human colorectal cancer (CRC) cell lines SW620, HCT116 and DLD-1 were purchased from Bioresource Collection and Research Center (BCRC, Taiwan) and grown in RPMI-1640 media (Cytiva) with 10% FBS. Human umbilical vein endothelial cells (HUVEC) were purchased from Sigma (200-05 N) and maintained in endothelial cell growth medium (Sigma). Human colonic epithelial cell line CCD 841 CoN, CRC cell line HT29, monocyte THP-1, and HEK 293T cells were from American Type Culture Collection (ATCC). CCD 841 CoN cells were grown in ATCC-formulated Eagle's minimum essential medium with 15% FBS. HT29 cells were grown in RPMI-1640 with 10% FBS. THP-1 cells were cultured in RPMI-1640 medium supplemented with 10% FBS, 10 mM HEPES, 1 mM sodium pyruvate, 2.5 g/L glucose and 0.05 mM 2-mercaptoethanol. HEK 293T cells were cultured in DMEM with 10% FBS. All cells were cultured at 37 °C in a 5% CO_2 humidified atmosphere, with routine mycoplasma test.

Lentiviral transduction of Siglec-5 and Siglec-14 to THP-1 cells

HEK 293T cells were cotransfected with lentiviral packaging plasmids pCMVΔ8.91 and pMG2.G and pLVX-EF1α-IRES-Puro empty vector (TaKaRa), pLVX-Siglec-5, or pLVX-Siglec-14 using Lipofectamine™ 3000 (Thermo Fisher). After a 16-h incubation, the media was changed to DMEM with 10% FBS. Lentivirus-containing supernatants were collected after 72 h of incubation, centrifuged at 1600 rpm for 10 min, filtered, concentrated and stored at −80 °C until used. THP-1 cells were infected with these lentiviral preparations, and selected with puromycin (2 μg/ml) for 1 week. The selected THP-1 cells were stained with APC-conjugated anti-human CD170 antibodies (BioLegend, clone 1A5) and sorted with BD FACSAria (BD Biosciences) through the service provided by the Flow Cytometric Analyzing and Sorting Core (the First Core Laboratory, National Taiwan University College of Medicine).

Preparation of tumor-conditioned medium (TCM)

To generate CRC TCM and normal colonic epithelial cell conditioned medium, SW620, HT29, HCT116, DLD-1, and CCD 841 CoN cells were cultured in a 10-cm dish until ~90% confluence. The medium was then replaced with fresh serum-free RPMI-1640 medium, and cells were cultured for 48 h at 37 °C. The conditioned medium was collected by centrifuging at 1600 rpm for 10 min, filtered through 0.22-μm filters, and stored at −80 °C until used. To generate sialic acid-deficient TCM, TCM was collected from SW620 CMAS-knockout cells or from SW620 cells treated with the sialyltransferase inhibitor P-3Fax-Neu5Ac (R&D System) for 2 days.

THP-1 differentiation and polarization

THP-1 cells (10^6 cells/ml) were treated with 100 nM phorbol 12-myristate 13-acetate (PMA) for 24 h to induce differentiation into macrophage. PMA-differentiated THP-1 macrophages were then polarized into M1 macrophages with IFN-γ (BioLegend, 20 ng/ml) and LPS (Sigma, 100 ng/ml) for 24 h, or into M2 macrophages with IL-4 (BioLegend, 20 ng/ml) and IL-13 (BioLegend, 20 ng/ml) for 48 h, unless otherwise specified. To generate TAMs, PMA-differentiated THP-1 macrophages were treated with 50% TCM, prepared as a 50:50 mixture of TCM and RPMI-1640 medium containing 2% FBS, for 48 h. The supernatants from these TCM-treated macrophages were collected and designated as macrophage-conditioned medium (MφCM) for subsequent experiments. To investigate the role of spleen tyrosine kinase (SYK) and Siglec-14 in TAM polarization, the SYK inhibitor BAY 61-3606 (MedChemExpress) and Siglec-5/14 neutralizing antibodies (clone 1A5, BioLegend) were added during TCM-induced TAM polarization, as specified in the legend.

RNA isolation and qRT-PCR

Total cellular RNA from mammalian cells was isolated with NucleoZol reagent (Macherey-Nagel) and transcribed to cDNA using PrimeScript™ RT reagent Kit (TaKaRa). RT-qPCR was performed on a CFX96 Touch™ Real-time PCR detection system (Bio-Rad) using qPCRBIO SyGreen® Blue Mix (PCR Biosystems) to quantify the expression of target genes. The expression levels were normalized to *HPRT1*. The primers used for RT-qPCR are listed in Supplementary Table 1.

Cytokine analysis

Cytokine levels in cell culture supernatants were quantified using CCL22, VEGF, and Galectin-3BP DuoSet ELISA kits from R&D Systems and TNF-α, IL-1β, and IL-6 ELISA kits from Thermo Fisher.

RNA-sequencing and data analysis

PMA-differentiated THP-1 macrophages were treated with 50% SW620 TCM (TCM^{SW620}) for 48 h. Total cellular RNA was isolated using NucleoZol and used for the preparation of the sequencing library by TruSeq Stranded mRNA Library Prep Kit (Illumina). Briefly, mRNA was purified from total RNA (1 μg) by oligo(dT)-coupled magnetic beads and fragmented into small pieces under elevated temperature. The first-strand cDNA was synthesized using reverse transcriptase and random primers. After the generation of double-strand cDNA and adenylation on the 3' ends of DNA fragments, the adapters were ligated. The products were enriched with PCR and purified with the AMPure XP system (Beckman Coulter). The libraries were qualified by the Qsep400 System (Bioptic Inc., Taiwan) and quantified by Qubit 2.0 Fluorometer (Thermo Scientific). The qualified libraries were

then sequenced on an Illumina NovaSeq platform with 150 bp paired-end reads generated by Genomics, BioSci & Tech Co. (Taiwan).

Sequencing data were trimmed using Fastp, and the processed reads were aligned to the human reference genome (GRCh38) using HISAT2 to generate the expression profile. Differential expression analysis was conducted with DESeq2, considering genes with an adjusted *p* value (*p* adj) <0.05 as statistically significant. Unbiased Gene Set Enrichment Analysis (GSEA) was performed using Gene Ontology (GO) enrichment analysis, Kyoto Encyclopedia of Genes and Genomes (KEGG) pathways, and the MSigDB (v7.0) hallmark gene sets to identify activated pathways and hallmark gene sets enriched in the high-abundance group. The GO enrichment analysis for cluster-specific gene was performed using the Database for Annotation, Visualization, and Integrated Discovery (DAVID)[71,72]. An expression heatmap comparing $SPP1^+$ and $C1QC^+$ macrophage signatures across groups was generated using Heatmapper[73].

In vivo tumor xenograft model

Six-week-old BALB/cAnN.Cg-*Foxn1nu*/CrlNarl mice (purchased from National Laboratory Animal Center, Taiwan) were housed in a daily cycle of 12 h light and 12 h darkness under pathogen-free conditions. A total of 10^6 SW620 cells alone or mixed with 3×10^6 PMA-differentiated THP-1 macrophages were subcutaneously inoculated into the right flank of the mice. Tumor volume of each mouse was measured twice per week under inhalation anesthesia with 2% isoflurane delivered in oxygen. Tumor size was calculated using the formula: volume = (length × width^2)/2. On day 31, all mice were euthanized by CO_2 inhalation (flow rate 30–70% of chamber volume per minute). Tumors were subsequently excised, photographed, and weighed.

Endothelial survival assay

HUVECs were seeded in 96-well tissue culture plates at 5×10^4 cells/well for 24 h, rinsed with HBSS and replaced with 200 µl of 50% MφCM, a 50/50 mix of the MφCM and endothelial cell basal medium (Sigma) with 2% FBS. After 48 h of incubation, cells were rinsed and incubated with WST-1 (TaKaRa)-containing fresh medium for 2 h. Absorbance of each well was measured at 450 nm by a spectrophotometer.

Transwell migration assay

The migration of HUVEC was analyzed using a 24-well hanging cell insert with 8-µm pores (JET Biofil). HUVECs (10^5 cells/well) were suspended in serum-free endothelial cell basal medium and added into the upper chamber, while the lower chamber was supplied with 400 µl of endothelial cell basal medium or 50% MφCM. After incubation for 24 h, non-migrated cells were scraped off from the upper surface with a cotton swab. The migrated cells were fixed in 4% paraformaldehyde for 30 min at room temperature, stained with 0.5% crystal violet for 20 min and counted under a microscope.

Tube formation assay

HUVECs (1.5×10^4) were suspended in 100 µl either endothelial cell basal medium or 50% MφCM and seeded onto a 96-well plate pre-coated with Geltrex™ basement membrane matrix (Thermo Fisher). After incubation at 37 °C for 6 h, images were taken and analyzed using the Angiogenesis Analyzer plugin in ImageJ to determine the number of meshes and segments.

Chorioallantoic membrane (CAM) assay

The CAM assay was performed as described previously[74] with minor modifications. Fertilized chicken eggs were purchased from SFP chicken farm (JD-SFP Biotech, Taiwan), and incubated horizontally at 37 °C in a 70% humidified egg incubator. On embryo development day (EDD) 3, ~6 ml of albumin was aspirated to detach the developing CAM from the top part of the shell, and a window of ~4 cm^2 was made on the wide end of the egg and sealed with a Tegaderm™ transparent film (3 M) to prevent dehydration. On EDD 6, eggs with exposed CAM were incubated with a 6 mm sterilized filter disc containing 15 µl of tenfold concentrated control RPMI medium or MφCM collected from TCM^{SW620}-treated THP-1 macrophages. After a further incubation for 3 days, the CAM was fixed with 10% formalin and photographed by a stereomicroscope (Olympus SZX7) at 16x magnification. The contrast of images was slightly adjusted to clearly show the microvessels. The number of vessel branching points and segments in each CAM are quantified by the WimCAM image analysis tool (Onimagen Technologies).

Western blot

Cells were lysed in ice-cold lysis buffer (50 mM Tris-HCl, 150 mM NaCl, 1% NP-40 with Halt™ Protease and Phosphatase Inhibitor Cocktail (Thermo Fisher)). The protein concentration was measured with a Pierce™ BCA Protein Assay Kit (Thermo Fisher). The collected cell lysate (60 µg) was separated on 10% SDS-PAGE, transferred to the PVDF membrane (Cytiva), probed with indicated antibodies or lectins listed in Supplementary Table 2, and visualized with a LI-COR Odyssey scanner after addition of IRDye® 800CW- or 680RD-conjugated secondary antibodies (LI-COR).

Expression and purification of Siglec-Fc chimeric proteins

Wild-type and Sia-binding-deficient R119A mutant variants of Siglec-5-Fc and Siglec-14-Fc chimeric proteins were expressed and purified based on previously established protocols with slight modifications[24,69]. Briefly, Siglec-Fc constructs in pcDNA3.1 vectors (from Dr. Takashi Angata, Academia Sinica) were transfected into HEK 293T cells using Lipofectamine™ 3000. After a 16-h incubation, the medium was changed with a 50:50 mixture of serum-free DMEM and RPMI-1640 supplemented with 2 mM L-glutamine, 2 mM sodium pyruvate and 1% HL-1™ Supplement (Lonza). The cells were cultured for an additional 48 h, and the culture supernatants were collected. The medium replacement and culture process were repeated to collect additional supernatants after another 48 h. The combined supernatants were processed to purify Siglec-Fc proteins using rProtein A Sepharose™ Fast Flow resins (Cytiva). The bound Siglec-Fc proteins were washed thoroughly with Tris-buffered saline (TBS; 20 mM Tris-HCl, 150 mM NaCl, pH 8.0), and subsequently treated with neuraminidase from *Arthrobacter ureafaciens* (EY Laboratories) for 1 h at room temperature to remove Sias. After extensive washing with TBS, the Siglec-Fc were eluted with 0.1 M glycine-HCl, pH 3.0, immediately neutralized with 1 M Tris-HCl buffer, pH 8.0 and concentrated using Amicon Ultra centrifugal filters (Merck).

ELISA for Siglec-TCM^{SW620} interaction

A 96-well plate was coated with 100 µl of a 50-fold diluted TCM^{SW620} in 50 mM sodium carbonate/bicarbonate buffer (pH 9.6) and incubated overnight at 4 °C. The wells were washed with TBS, blocked with 2% BSA/TBS for 1 h at room temperature, and incubated with 0.1 µg of wild-type or R119A Siglec-Fc (diluted in 100 µl of 2% BSA/TBS) for 2 h at room temperature. After incubation, the wells were washed with TBS and incubated with biotinylated goat $F(ab')^2$ anti-human IgG (SouthernBiotech) for 30 min. After washing again with TBS, horseradish peroxidase (HRP)-conjugated streptavidin was added and incubated for 30 min. Following extensive TBS washing, HRP activity was developed with TMB substrate (BioLegend) for 20 min. The reaction was stopped by adding H_2SO_4, and the absorbance was measured at 450 nm using a spectrophotometer.

Immunoprecipitation

Wild-type and R119A Siglec-14-Fc proteins (5 µg each) were incubated with rProtein A Sepharose™ Fast Flow resins at room temperature for 2 h. After washing, the resin complexes were incubated with 1 ml of TCM^{SW620} overnight at 4 °C with rotation. The resins were subsequently washed three times with TBST (TBS with 0.1% Tween-20), followed by incubation with TBS supplemented with 3 mM 3'-sialyllactose and 3 mM 6'-sialyllactose (Biosynth) at room temperature for 45 min to elute the bound sialylated ligands. The eluted proteins were resolved on an

SDS-PAGE gel, visualized using a Silver Stain Plus Kit (Bio-Rad) and identified via mass spectrometry.

LC-MS/MS analysis

Proteins eluted from Siglec-Fc proteins were reduced with 10 mM dithiothreitol for 30 min at 37 °C, followed by alkylation with iodoacetamide at a final concentration of 50 mM for 45 min at 37 °C in the dark. Proteins were then digested with trypsin (Promega) at a 1:50 (w/w) enzyme-to-substrate ratio overnight at 37 °C. The resulting tryptic peptides were acidified to pH 2–3 using TFA and desalted with Zip Tip® pipette tips (Merck). Tryptic peptides were analyzed using an Orbitrap Fusion Lumos mass spectrometer (Thermo Scientific) coupled with a Thermo Scientific UltiMate 3000 RSLCnano system (Thermo Scientific).

Peptide mixtures were loaded onto a Thermo Scientific PepMap C18 column (25 cm × 75 μm ID, Thermo Scientific) and separated using a gradient from 4 to 38.5% solvent B (ACN with 0.1% formic acid) over 90 min at a flow rate of 300 nL/min with the column temperature of 40 °C. Solvent A was 0.1% formic acid in water. The mass spectrometer operated in TopSpeed mode with a cycle time of 3 s. Full-scan MS spectra were acquired in the Orbitrap (m/z 375–1500) with a resolution of 60,000, an automatic gain control (AGC) target of 4e5, and a maximum injection time (IT) of 50 ms. The most intense ions were sequentially isolated for HCD MS/MS fragmentation and detected in the Orbitrap with dynamic exclusion for 20 s. For MS/MS, the resolution was set to 30,000, the isolation window was 1.4 Th, and the AGC target was set as 5e4, and maximum IT was 54 ms. Fragmentation was performed with a normalized collision energy of 30%. The precursor ions with 2+ to 7+ charges were selected for HCD fragmentation.

Data processing

All MS raw files were processed with MaxQuant (ver. 1.6.14.0) by the Andromeda engine against the SwissProt *Homo sapiens* database (downloaded on 2020.02) containing 20,303 protein entries, for protein identification and quantification. The search parameters included a precursor mass tolerance of 10 ppm and a product ion mass tolerance of 0.05 Da, with trypsin as the enzyme, allowing for up to two missed cleavages. Carbamidomethylation of cysteine (C, +57.021 Da) was set as a fixed modification, while oxidation of methionine (M, +15.995 Da) and acetylation of the protein N-terminus (protein N-term, +42.011 Da) were considered as variable modifications. A minimum peptide length of seven residues was required, and a false discovery rate (FDR) of 1% was applied to both peptide and protein identifications. Known contaminants were excluded for subsequent analysis.

CRISPR/Cas9 gene inactivation

LGALS3BP and CMAS sgRNAs (sequences listed in Supplementary Table 1) were cloned into the pSpCas9(BB)-2A-Puro (PX459) V2.0 plasmid[75]. The resulting constructs were transfected into SW620 cells using Lipofectamine™ 3000. Transfected cells were selected with puromycin (2 μg/ml) for 1 week, followed by single-clone isolation and expansion. Knockout efficiency was confirmed by Western blotting with antibodies listed in Supplementary Table 2.

Patient samples and follow-up data

This study included 357 patients with primary CRC undergoing surgery at Taipei Veterans General Hospital from 01/13/2014 to 12/27/2017. None of the patients had received radiotherapy and chemotherapy before the operation. These patients had detailed clinical information, including gender, histological type, cancer stage, and survival. The pathological stages were determined based on the American Joint Committee on Cancer (AJCC) TNM system, a standard classification system of the anatomical extent of cancers describing the size of the tumor (T), the extent of spread to the lymph nodes (N), and the presence of metastasis (M). Blood carcinoembryonic antigen (CEA) and carbohydrate antigen 19-9 (CA19-9) were obtained from routine blood tests at the time of surgery. The most recent follow-up was completed on 05/14/2024. CRC-specific survival (CSS) was defined as the time from the initial diagnosis of CRC to the unfortunate event of death caused by CRC.

Genotyping

Genomic DNA and sera were obtained from the Biobank of Taipei Veterans General Hospital. The collection and use of specimens comply with the Declaration of Helsinki. Genotyping of the *SIGLEC14* locus was performed as described previously with slight modification[27]. A set of three PCR reactions was run in parallel to specifically amplify the *SIGLEC14*, *SIGLEC5*, and *SIGLEC14/5* fusion genes. Primers used for specific amplification for *SIGLEC14*, *SIGLEC5*, and *SIGLEC14/5* fusion genes are listed in Supplementary Table 1. Thermal cycling parameters are as follows: 94 °C, 2 min; (94 °C, 30 s; 54 °C, 45 s; 72 °C, 1.5 min) × 27 cycles; 72 °C, 5 min.

Statistical analysis

Statistical analyses for the clinical data were performed using SPSS version 24 software. The χ^2 test and Student's *t*-test were used to evaluate associations among patient clinical characteristics. CRC-specific survival was analyzed using the Kaplan–Meier method, and the log-rank test was used to identify the differences between survival curves. Univariate and multivariate prognosis analyses were conducted with the Cox proportional hazards regression model using a forward stepwise procedure. Statistical tests for the in vitro and animal experiments were performed using GraphPad Prism version 9 software (GraphPad Software, Inc.). Data presented here were combined, normalized and expressed as mean ± SD. A p value less than 0.05 was considered statistically significant for all analyses.

Ethics approval

The human studies were approved by the Institutional Review Board of Taipei Veterans General Hospital (2021-02-015BC) and the Institutional Review Board of National Taiwan University Hospital (202101125RINB), and all study participants signed preapproved informed consent documents prior to enrollment into the studies. All the animal experiments were performed in accordance with relevant guidelines and regulations approved by the Institutional Animal Care and Use Committee of National Taiwan University College of Medicine (IACUC 20210289).

Data availability

All relevant data are presented in this paper. If any more information is needed, data are available from the corresponding author upon reasonable request. The RNA-seq dataset has been uploaded to NCBI Gene Expression Omnibus with the accession number GSE310306.

Received: 16 June 2025; Accepted: 20 October 2025;
Published online: 15 December 2025

References

1. Bray, F. et al. Global cancer statistics 2022: GLOBOCAN estimates of incidence and mortality worldwide for 36 cancers in 185 countries. *CA Cancer J. Clin.* **74**, 229–263 (2024).
2. Siegel, R. L., Wagle, N. S., Cercek, A., Smith, R. A. & Jemal, A. Colorectal cancer statistics, 2023. *CA Cancer J. Clin.* **73**, 233–254 (2023).
3. Bull, C., Stoel, M. A., den Brok, M. H. & Adema, G. J. Sialic acids sweeten a tumor's life. *Cancer Res.* **74**, 3199–3204 (2014).
4. Pinho, S. S. & Reis, C. A. Glycosylation in cancer: mechanisms and clinical implications. *Nat. Rev. Cancer* **15**, 540–555 (2015).
5. Rodrlguez, E., Schetters, S. T. T. & van Kooyk, Y. The tumour glycocode as a novel immune checkpoint for immunotherapy. *Nat. Rev. Immunol.* **18**, 204–211 (2018).
6. Stanczak, M. A. & Laubli, H. Siglec receptors as new immune checkpoints in cancer. *Mol. Asp. Med.* **90**, 101112 (2023).
7. van Houtum, E. J. H., Bull, C., Cornelissen, L. A. M. & Adema, G. J. Siglec signaling in the tumor microenvironment. *Front. Immunol.* **12**, 790317 (2021).

8. Angata, T. & Varki, A. Discovery, classification, evolution and diversity of Siglecs. *Mol. Asp. Med.* **90**, 101117 (2023).
9. Crocker, P. R., Paulson, J. C. & Varki, A. Siglecs and their roles in the immune system. *Nat. Rev. Immunol.* **7**, 255–266 (2007).
10. Beatson, R. et al. Cancer-associated hypersialylated MUC1 drives the differentiation of human monocytes into macrophages with a pathogenic phenotype. *Commun. Biol.* **3**, 644 (2020).
11. Beatson, R. et al. The mucin MUC1 modulates the tumor immunological microenvironment through engagement of the lectin Siglec-9. *Nat. Immunol.* **17**, 1273–1281 (2016).
12. Haas, Q. et al. Siglec-9 regulates an effector memory CD8(+) T-cell subset that congregates in the melanoma tumor microenvironment. *Cancer Immunol. Res.* **7**, 707–718 (2019).
13. Hudak, J. E., Canham, S. M. & Bertozzi, C. R. Glycocalyx engineering reveals a Siglec-based mechanism for NK cell immunoevasion. *Nat. Chem. Biol.* **10**, 69–75 (2014).
14. Jandus, C. et al. Interactions between Siglec-7/9 receptors and ligands influence NK cell-dependent tumor immunosurveillance. *J. Clin. Invest.* **124**, 1810–1820 (2014).
15. Rodriguez, E. et al. Sialic acids in pancreatic cancer cells drive tumour-associated macrophage differentiation via the Siglec receptors Siglec-7 and Siglec-9. *Nat. Commun.* **12**, 1270 (2021).
16. Stanczak, M. A. et al. Self-associated molecular patterns mediate cancer immune evasion by engaging Siglecs on T cells. *J. Clin. Invest.* **128**, 4912–4923 (2018).
17. Barkal, A. A. et al. CD24 signalling through macrophage Siglec-10 is a target for cancer immunotherapy. *Nature* **572**, 392–396 (2019).
18. Wu, Y. et al. Proximity labeling and genetic screening reveal that DSG2 is a counter receptor of Siglec-9 and suppresses macrophage phagocytosis. *Adv. Sci.* https://doi.org/10.1002/advs.202406654 (2025).
19. Huang, Z. et al. Siglec-15 on macrophages suppress the immune microenvironment in patients with PD-L1 negative non-metastasis lung adenocarcinoma. *Cancer Gene Ther.* **31**, 427–438 (2024).
20. Takamiya, R., Ohtsubo, K., Takamatsu, S., Taniguchi, N. & Angata, T. The interaction between Siglec-15 and tumor-associated sialyl-Tn antigen enhances TGF-beta secretion from monocytes/macrophages through the DAP12-Syk pathway. *Glycobiology* **23**, 178–187 (2013).
21. Wang, J. et al. Siglec-15 as an immune suppressor and potential target for normalization cancer immunotherapy. *Nat. Med.* **25**, 656–666 (2019).
22. Wang, Y. et al. Siglec-15/sialic acid axis as a central glyco-immune checkpoint in breast cancer bone metastasis. *Proc. Natl Acad. Sci. USA* **121**, e2312929121 (2024).
23. Thiesler, H. et al. Proinflammatory macrophage activation by the polysialic acid-Siglec-16 axis is linked to increased survival of patients with glioblastoma. *Clin. Cancer Res.* **29**, 2266–2279 (2023).
24. Angata, T., Hayakawa, T., Yamanaka, M., Varki, A. & Nakamura, M. Discovery of Siglec-14, a novel sialic acid receptor undergoing concerted evolution with Siglec-5 in primates. *FASEB J.* **20**, 1964–1973 (2006).
25. Ali, S. R. et al. Siglec-5 and Siglec-14 are polymorphic paired receptors that modulate neutrophil and amnion signaling responses to group B Streptococcus. *J. Exp. Med.* **211**, 1231–1242 (2014).
26. Angata, T. et al. Loss of Siglec-14 reduces the risk of chronic obstructive pulmonary disease exacerbation. *Cell Mol. Life Sci.* **70**, 3199–3210 (2013).
27. Yamanaka, M., Kato, Y., Angata, T. & Narimatsu, H. Deletion polymorphism of SIGLEC14 and its functional implications. *Glycobiology* **19**, 841–846 (2009).
28. Zhang, L. et al. Single-cell analyses inform mechanisms of myeloid-targeted therapies in colon cancer. *Cell* **181**, 442–459.e429 (2020).
29. Cheng, S. et al. A pan-cancer single-cell transcriptional atlas of tumor infiltrating myeloid cells. *Cell* **184**, 792–809.e723 (2021).
30. Rodrigues, E. et al. A versatile soluble siglec scaffold for sensitive and quantitative detection of glycan ligands. *Nat. Commun.* **11**, 5091 (2020).
31. Eng, C. et al. Atezolizumab with or without cobimetinib versus regorafenib in previously treated metastatic colorectal cancer (IMblaze370): a multicentre, open-label, phase 3, randomised, controlled trial. *Lancet Oncol.* **20**, 849–861 (2019).
32. Le, D. T. et al. PD-1 blockade in tumors with mismatch-repair deficiency. *N. Engl. J. Med.* **372**, 2509–2520 (2015).
33. Yin, J. et al. SIGLEC11 promotes M2 macrophage polarization through AKT-mTOR signaling and facilitates the progression of gastric cancer. *J. Immunother. Cancer* **13**, e010162 (2025).
34. Wieboldt, R. et al. Engagement of sialylated glycans with Siglec receptors on suppressive myeloid cells inhibits anticancer immunity via CCL2. *Cell Mol. Immunol.* **21**, 495–509 (2024).
35. Xiao, R. et al. Increased Siglec-9/Siglec-9L interactions on NK cells predict poor HCC prognosis and present a targetable checkpoint for immunotherapy. *J. Hepatol.* **80**, 792–804 (2024).
36. Yin, S. et al. Siglec-G suppresses CD8(+) T cells responses through metabolic rewiring and can be targeted to enhance tumor immunotherapy. *Adv. Sci.* **11**, e2403438 (2024).
37. Xiao, H., Woods, E. C., Vukojicic, P. & Bertozzi, C. R. Precision glycocalyx editing as a strategy for cancer immunotherapy. *Proc. Natl Acad. Sci. USA* **113**, 10304–10309 (2016).
38. Gray, M. A. et al. Targeted glycan degradation potentiates the anticancer immune response in vivo. *Nat. Chem. Biol.* **16**, 1376–1384 (2020).
39. Laubli, H. et al. Engagement of myelomonocytic Siglecs by tumor-associated ligands modulates the innate immune response to cancer. *Proc. Natl Acad. Sci. USA* **111**, 14211–14216 (2014).
40. Friedman, D. J. et al. ST8Sia6 promotes tumor growth in mice by inhibiting immune responses. *Cancer Immunol. Res.* **9**, 952–966 (2021).
41. Schmassmann, P. et al. Targeting the Siglec-sialic acid axis promotes antitumor immune responses in preclinical models of glioblastoma. *Sci. Transl. Med.* **15**, eadf5302 (2023).
42. Stanczak, M. A. et al. Targeting cancer glycosylation repolarizes tumor-associated macrophages allowing effective immune checkpoint blockade. *Sci. Transl. Med.* **14**, eabj1270 (2022).
43. Wu, J. et al. Targeted glycan degradation potentiates cellular immunotherapy for solid tumors. *Proc. Natl Acad. Sci. USA* **120**, e2300366120 (2023).
44. Liu, Q., Xing, H., Xiong, M. & Zhang, X. B. Specifically editing cancer sialoglycans for enhanced in vivo immunotherapy through aptamer-enzyme chimeras. *Angew. Chem. Int. Ed. Engl.* **64**, e202414327 (2025).
45. Sasaki, T., Brakebusch, C., Engel, J. & Timpl, R. Mac-2 binding protein is a cell-adhesive protein of the extracellular matrix which self-assembles into ring-like structures and binds beta1 integrins, collagens and fibronectin. *EMBO J.* **17**, 1606–1613 (1998).
46. Muller, S. A. et al. Domain organization of Mac-2 binding protein and its oligomerization to linear and ring-like structures. *J. Mol. Biol.* **291**, 801–813 (1999).
47. Laferte, S. & Loh, L. C. Characterization of a family of structurally related glycoproteins expressing beta 1-6-branched asparagine-linked oligosaccharides in human colon carcinoma cells. *Biochem. J.* **283**, 193–201 (1992).
48. Iacobelli, S. et al. Purification and characterization of a 90 kDa protein released from human tumors and tumor cell lines. *FEBS Lett.* **319**, 59–65 (1993).
49. Koths, K., Taylor, E., Halenbeck, R., Casipit, C. & Wang, A. Cloning and characterization of a human Mac-2-binding protein, a new member of the superfamily defined by the macrophage scavenger receptor cysteine-rich domain. *J. Biol. Chem.* **268**, 14245–14249 (1993).

50. Laubli, H. et al. Lectin galactoside-binding soluble 3 binding protein (LGALS3BP) is a tumor-associated immunomodulatory ligand for CD33-related Siglecs. *J. Biol. Chem.* **289**, 33481–33491 (2014).
51. Cao, H. et al. SIGLEC16 encodes a DAP12-associated receptor expressed in macrophages that evolved from its inhibitory counterpart SIGLEC11 and has functional and non-functional alleles in humans. *Eur. J. Immunol.* **38**, 2303–2315 (2008).
52. Schwarz, F. et al. Paired Siglec receptors generate opposite inflammatory responses to a human-specific pathogen. *EMBO J.* **36**, 751–760 (2017).
53. Landig, C. S. et al. Evolution of the exclusively human pathogen Neisseria gonorrhoeae: human-specific engagement of immunoregulatory Siglecs. *Evol. Appl.* **12**, 337–349 (2019).
54. Sun, J. et al. Exploring the cross-cancer effect of circulating proteins and discovering potential intervention targets for 13 site-specific cancers. *J. Natl Cancer Inst.* **116**, 565–573 (2024).
55. Shi, H., Gao, L., Zhang, W. & Jiang, M. Identification and validation of a siglec-based and aging-related 9-gene signature for predicting prognosis in acute myeloid leukemia patients. *BMC Bioinformatics* **23**, 284 (2022).
56. Huang, P. J., Low, P. Y., Wang, I., Hsu, S. D. & Angata, T. Soluble Siglec-14 glycan-recognition protein is generated by alternative splicing and suppresses myeloid inflammatory responses. *J. Biol. Chem.* **293**, 19645–19658 (2018).
57. Ovsyannikova, I. G. et al. Genome-wide determinants of cellular immune responses to mumps vaccine. *Vaccine* **41**, 6579–6588 (2023).
58. Shaw, B. C., Katsumata, Y., Simpson, J. F., Fardo, D. W. & Estus, S. Analysis of genetic variants associated with levels of immune modulating proteins for impact on Alzheimer's disease risk reveal a potential role for SIGLEC14. *Genes* https://doi.org/10.3390/genes12071008 (2021).
59. Stampolidis, P., Ullrich, A. & Iacobelli, S. LGALS3BP, lectin galactoside-binding soluble 3 binding protein, promotes oncogenic cellular events impeded by antibody intervention. *Oncogene* **34**, 39–52 (2015).
60. Tinari, N. et al. Glycoprotein 90K/MAC-2BP interacts with galectin-1 and mediates galectin-1-induced cell aggregation. *Int. J. Cancer* **91**, 167–172 (2001).
61. Becker, R. et al. Tumor stroma marker endosialin (Tem1) is a binding partner of metastasis-related protein Mac-2 BP/90K. *FASEB J.* **22**, 3059–3067 (2008).
62. Lee, J. H. et al. Glycoprotein 90K, downregulated in advanced colorectal cancer tissues, interacts with CD9/CD82 and suppresses the Wnt/beta-catenin signal via ISGylation of beta-catenin. *Gut* **59**, 907–917 (2010).
63. Nonaka, M. et al. Dendritic cell-specific intercellular adhesion molecule 3-grabbing non-integrin (DC-SIGN) recognizes a novel ligand, Mac-2-binding protein, characteristically expressed on human colorectal carcinomas. *J. Biol. Chem.* **286**, 22403–22413 (2011).
64. Shahraz, A. et al. Anti-inflammatory activity of low molecular weight polysialic acid on human macrophages. *Sci. Rep.* **5**, 16800 (2015).
65. Macauley, M. S., Crocker, P. R. & Paulson, J. C. Siglec-mediated regulation of immune cell function in disease. *Nat. Rev. Immunol.* **14**, 653–666 (2014).
66. Tsubata, T. Siglec cis-ligands and their roles in the immune system. *Glycobiology* **33**, 532–544 (2023).
67. Lin, S. Y., Schmidt, E. N., Takahashi-Yamashiro, K. & Macauley, M. S. Roles for Siglec-glycan interactions in regulating immune cells. *Semin. Immunol.* **77**, 101925 (2024).
68. Gonzalez-Gil, A. & Schnaar, R. L. Siglec ligands. *Cells* https://doi.org/10.3390/cells10051260 (2021).
69. Fong, J. J. et al. Immunomodulatory activity of extracellular Hsp70 mediated via paired receptors Siglec-5 and Siglec-14. *EMBO J.* **34**, 2775–2788 (2015).
70. Suematsu, R. et al. Identification of lipophilic ligands of Siglec5 and -14 that modulate innate immune responses. *J. Biol. Chem.* **294**, 16776–16788 (2019).
71. Huang da, W., Sherman, B. T. & Lempicki, R. A. Systematic and integrative analysis of large gene lists using DAVID bioinformatics resources. *Nat. Protoc.* **4**, 44–57 (2009).
72. Sherman, B. T. et al. DAVID: a web server for functional enrichment analysis and functional annotation of gene lists (2021 update). *Nucleic Acids Res.* **50**, W216–W221 (2022).
73. Babicki, S. et al. Heatmapper: web-enabled heat mapping for all. *Nucleic Acids Res.* **44**, W147–W153 (2016).
74. Luh, H. T. et al. Does a negative correlation of heme oxygenase-1 with hematoma thickness in chronic subdural hematomas affect neovascularization and microvascular leakage? A retrospective study with preliminary validation. *J. Neurosurg.* **139**, 536–543 (2023).
75. Ran, F. A. et al. Genome engineering using the CRISPR-Cas9 system. *Nat. Protoc.* **8**, 2281–2308(2013).

Acknowledgements

This work was supported by grants from the Ministry of Education in Taiwan, National Taiwan University (NTU-CC-111L893902, 112L892702, 113L890902, 114L894102). We thank Dr. Ruby Y-J Huang (National Taiwan University) for her guidance on CAM analysis. We also thank Dr. Takashi Angata (Academia Sinica) for providing the Siglec-Fc expression constructs, Dr. Shu-Jung Chang (National Taiwan University) for the PX459 plasmid, and the National RNAi core facility for the lentiviral packaging plasmids (pCMVΔ8.91 and pMG2.G). We are grateful for the technical support provided by the Animal Core Facility, Department of Medical Research, National Taiwan University Hospital and the Flow Cytometric Analyzing and Sorting Core of the First Core Laboratory, National Taiwan University, College of Medicine. We thank the Glycan Sequencing Core and Mass Spectrometry Core, Genomics Research Center, Academia Sinica, for performing the glycan analyses.

Author contributions

K.-Y.L., J.-I.L., S.-Y.L., and Y.-C.K. performed experiments, analyzed data and prepared materials for the manuscript. J.-K.J. and C.-Y.Y. supplied the CRC samples and supervised the clinical data analysis. L.-C.L. conducted the clinical data analysis. M.-H.L. conducted mass spectrometry analysis. T.-L.H. conducted the glycan mass spectrometry analysis. Y.-C.C. designed and supervised experiments, interpreted data, conceptualized the study, and wrote the manuscript with all authors providing critical input and edits.

Competing interests

The authors declare no competing interests.

Additional information

Supplementary information The online version contains supplementary material available at https://doi.org/10.1038/s41698-025-01169-0.

Correspondence and requests for materials should be addressed to Yung-Chi Chang.